Tuning nonequilibrium colloidal structure in external fields by density-dependent state switching

Lennart Heinen [1], Sébastien Groh,[1] and Joachim Dzubiella [1,2,*]

[1]*Applied Theoretical Physics–Computational Physics, Physikalisches Institut, Albert-Ludwigs-Universität Freiburg, 79104 Freiburg, Germany*

[2]*Cluster of Excellence livMatS @ FIT-Freiburg Center for Interactive Materials and Bioinspired Technologies, Albert-Ludwigs-Universität Freiburg, 79110 Freiburg, Germany*

(Received 23 May 2024; accepted 22 July 2024; published 16 August 2024)

Biological cells have the ability to switch internal states depending on the density of other cells in their local environment, referred to as "quorum sensing." The latter can be utilized to control collective structuring, such as in biofilm formation. In this work, we study a simple quorum sensing model of ideal (noninteracting) colloids with a switchable internal degree of freedom in the presence of external potentials. The colloids have two possible discrete states, in which they are affected differently by the external field, and switch with rates dependent on the local density in their environment. We study this model with reactive Brownian dynamics simulations, as well as with an appropriate reaction-diffusion theory. We find remarkable structuring in the system controlled by the density-mediated interactions between the ideal colloids. We report results of different functional forms for the rate dependence and quantify the influence of their parameters, in particular, discuss the role of the *spatiotemporal sensing range*, i.e., how the resulting structures depend on how the environmental information is "measured" by the colloids. Especially in the case of a rate function with sigmoidal dependence on local density, i.e., requiring a threshold density for switching, we observe significant correlation effects in the density profiles which are tuneable by the sensing ranges but also sensitive to noise and fluctuations. Hence, our model gives some basic insights into the nonequilibrium structuring mediated by simple quorum sensing protocols.

DOI: 10.1103/PhysRevE.110.024604

I. INTRODUCTION

Quorum sensing is a signaling process that enables bacteria to communicate and coordinate collective behavior in dependence of the local cell population density [1–3]. Chemically, the cells emit and sense molecular (auto)inducers. Their detection triggers a different gene expression inside the cells with various behavioral consequences. For example, in the *Vibrio fisheri* bacteria [4–6], found in the Hawaiian squid, the quorum sensing process enables bioluminescence. In another scenario, quorum sensing triggers the expression of genes involved in the production of extracellular matrix components, which tune mobility as well as physical cell-cell interactions, and is therefore key for migration, structuring, and forming various biofilm architectures [7–9].

Understanding how quorum sensing drives the spatiotemporal collective structuring, e.g., in biofilm formation is crucial for developing effective strategies to prevent, control, and eliminate these persistent microbial communities which are often resistent to antibiotics. Because as fascinating as they may be, they lead to problems everywhere their growth is unwanted, especially in the context of biofouling of medical devices [10–12], like catheters or artificial joints. However, understanding and controlling these processes from the perspective of complex and colloidal fluids could potentially lead to the physics-based design and synthesis of active functional materials [13–18].

From a physical perspective, biofilm formation can be understood in the simplest terms as a directed self-assembly and adhesion of active macromolecules [14,19–21]. Hence, colloids, suspended particles in a liquid phase, which actively switch properties and interactions may serve as a simplified representation of microbial populations. Recently, for example, Alston *et al.* [20] presented a microscopic model inspired by the bacteria *Neisseria meningitidis* in which diffusive colloidal-like agents feel intermittent attractive forces. They demonstrated the presence of microphase separation where the colloidal cluster sizes were tuneable by the switching rate between particle states. Similarly, some of us explored theoretically the microstructure and phase behavior of soft colloids which can actively switch their interactions at a predefined kinetic rate [19,22]. They showed that sufficiently fast switching impedes the phase separation of an (in equilibrium) unstable liquid in both bulk and confinement, allowing the control of the degree of mixing, condensation, and local microstructuring in a cellular confinement by tuning the switching rate.

However, quorum sensing mediated structuring is based on communication and switching behavior depending on the local cell population density [15]. The influence of density-dependent communication and state-switching on colloidal structuring is unexplored, to the best of our knowledge. In this study, we fill this knowledge gap by investigating a simple model of colloids with local density-dependent properties, using particle-based simulations and reaction-diffusion

*Contact author: joachim.dzubiella@physik.uni-freiburg.de

theories. Similar methods haven been employed recently to study structuring by density-dependent diffusion and motility [17]. We keep our model as simple as possible and consider ideal, noninteracting (and nonmotile) colloids in which behavioral switching is accounted for by an internal degree of freedom, or "state" of the colloids, which either takes the discrete value a or b. We assume that the colloids are affected by an external potential originating from a possible biofilm host. The interaction with the potential depends on the colloid state and therefore conditions the different behavior observed for different gene expressions. The colloids switch their state based on switching rates k_{ab} and k_{ba}. We integrate the quorum sensing process into our model by making the switching rates dependent on the local density. We then systematically examine in our work the different possibilities of "measuring" or "sensing" the local density by the cells and the functional form of the switching rate dependence, and how they tune the resulting structures.

Our approach involves both Brownian dynamics (BD) simulations and a theoretical analysis to unravel the emergent behaviors of our model system. The theoretical description of our model is based on a reactive, overdamped Smoluchowski transport equation, but adapted to include the density-dependent reactive switching between states of the colloids. The two different perspectives and mutual comparisons enable us to develop a thorough understanding of the inner mechanisms of the colloid behavior.

This work is structured as follows. The first section introduces to our quorum sensing model and the used methods, namely the BD simulations and the theoretical framework. Afterwards, our results are presented, divided into constant rate studies, the influence of introducing the local density dependence and finally a description of the structural correlation effect we observe for a sigmoidal switching rate dependence. The final section summarizes our findings and concludes our studies.

II. MODEL AND METHODS

A. Switching colloid model

We consider a binary system of N ideal (noninteracting) colloids suspended in a liquid phase. Each particle $i = 1, .., N$ is characterized by a three-dimensional position vector $\vec{r}_i = (x_i, y_i, z_i)$ and an internal state $s = a, b$. Their movement is limited by two walls in the x direction, where the colloid-wall interaction is dependent on the internal state. The generic Mie-93 potential [23,24] is chosen for the interaction between the colloids and the wall in the form

$$\Phi_{93}(x; s) = \frac{3\sqrt{3}}{2}\epsilon\left[\left(\frac{\sigma}{x}\right)^9 - f(s)\left(\frac{\sigma}{x}\right)^3\right]. \tag{1}$$

Here, we introduced a switching function

$$f(s) = \begin{cases} 1 & \text{if } s = a, \\ 0 & \text{if } s = b, \end{cases} \tag{2}$$

which leads to colloidal attraction in state a, while repulsion only in state b. The attraction range σ sets the unit length in our model. The energy scale $\epsilon = 1\ k_BT$ sets the energy scale. An illustration of the model is provided in Fig. 1.

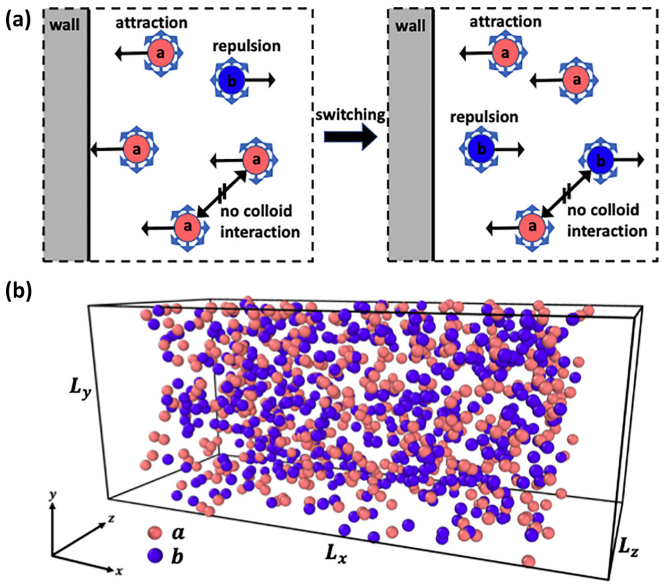

FIG. 1. Model and simulation snapshots. (a) Colloids in state a (red/light gray) are attracted to the wall. They can stochastically switch by a model-defined rate to state b (blue/dark gray) which is repulsive only. The colloids are mutually noninteracting (ideal). (b) Snapshot from the Brownian Dynamics simulations. Visible are $N = 1000$ colloids, distributed in the simulation box with dimensions $L_x = 10\sigma$, $L_y = L_z = 5\sigma$. The origin of the coordinate system is in the center of the simulation box. Two walls interacting with state-dependent potential given by Eq. (1) bound the system in the x direction.

The colloids change their internal state with the stochastic switching rates k_{ab} and k_{ba}. As a reference, we also investigate position-independent switching rates, but focus in this study on rates dependent on the local density of neighboring colloids, hence becoming a function of position. This captures implicitly the environmental effects of quorum sensing, e.g., between bacteria, in an effective and efficient way, especially because the functional form of the dependence can be adapted accordingly. In this way, the chemical autoinducer signaling molecules, that control the quorum sensing interactions in bacterial populations do not have to be modeled explicitly.

In the case of local density-dependent switching rates, we study the effects of linear and sigmoidal dependent functions (see Fig. 2), based on the following motivation: We want to impose that the general trend of the dependence has to be increasing for k_{ba}, so that bacteria with many neighbors favor state a, in which a biofilm can be initiated, and decreasing for k_{ab}, so that for low local density, the initial reference state b is favored. We express this by a strictly increasing k_+ and decreasing k_- and setting $k_{ba} = k_+$ and $k_{ab} = k_-$. The most simple expression of this trend is a linear dependence of the rate on the local density, where the slope is controlled by a free parameter k_{amp}:

$$k_\pm(x) = k_{\text{init}} \pm k_{\text{amp}} \cdot \left[\frac{\rho_{\text{loc}}(x)}{\rho_{\text{tot}}}\right]. \tag{3}$$

The local density, $\rho_{\text{loc}}(x)$, to be defined in detail below, is normalized with the total density of N colloids in the simulation volume V, namely $\rho_{\text{tot}} = N/V$. The amplitude k_{amp} simply

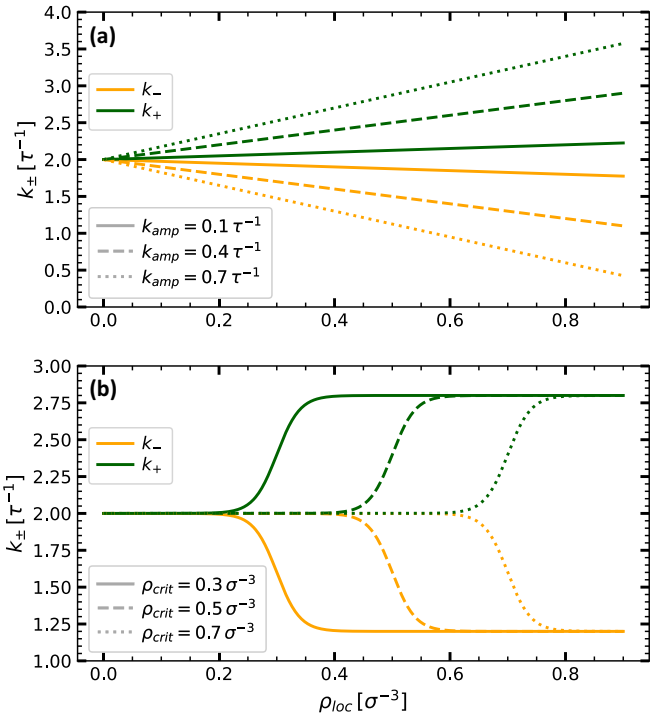

FIG. 2. Examples of the functional forms for the dependence of the position-dependent switching rates k_- (orange/light gray) and k_+ (green/dark gray) on the measured local colloid density ρ_{loc}. (a) Linear dependence functions for different amplitudes k_{amp}, see Eq. (3). (b) Sigmoidal dependence functions for different critical densities ρ_{crit}, see Eq. (4).

describes how strongly the rate scales with the local density, and k_{init} is a position-independent offset defining the ratio between populations a and b in the homogenous system. We note also that in crowding situations it was found theoretically that internal switching rates of elastically bistable colloids depend linearly on the local density for not too high densities [25]. Examples for $k(\rho_{\mathrm{loc}}(x))$ for different values of k_{amp} are shown in Fig. 2(a).

The sigmoidal dependence of rates on local density is well motivated from biology: In quorum sensing, it is common for bacteria to collectively change their behavior at a certain threshold density [15]. Because of the autoinducer production and their reflux back to a bacteria cell, there is a characteristic internal autoinducer concentration present. If the local density of neighboring bacteria exceeds a critical value, then this internal concentration is raised to a critical value and a different gene expression is triggered. We capture this behavior with a sigmoidal dependence function:

$$k_\pm(x) = k_{\mathrm{init}} \pm k_{\mathrm{amp}}\left[1 + e^{-\alpha_{\mathrm{sig}}\left(\frac{\rho_{\mathrm{loc}}(x)-\rho_{\mathrm{crit}}}{\rho_{\mathrm{tot}}}\right)}\right]^{-1}. \tag{4}$$

It contains the critical density ρ_{crit} as an additional parameter which sets the threshold for switching, as well as the parameter α_{sig} to control the transition sharpness. Example functions for different ρ_{crit} are plotted in Fig. 2(b).

B. Brownian dynamics simulations

In our BD simulations, $N = 100$ up to 1000 colloids diffuse in a box with dimensions of $L_x = 10\sigma$, and $L_y = L_z = 2.5\sigma$ to 5σ depending on total density. The origin of our coordinate system is placed in the center of the simulation box. The walls are placed in the x direction at $\pm L_x/2$. In the y and z directions periodic boundary conditions are applied. Figure 1(b) shows an example configuration of the simulation setup. We consider total densities in our systems in the range $\rho_{\mathrm{tot}} = N/(L_x L_y L_z) = 0.4\sigma^{-3}$ to $16\sigma^{-3}$.

Initially, the colloids are distributed randomly in the simulation box and an equilibration run is performed until a stationary distribution is reached. In a subsequent production run, the colloid positions and their states are saved for further analysis.

The colloid positions for a particle in state $s = a, b$ are updated every time step Δt according to standard overdamped Langevin dynamics [26]:

$$\vec{r}_i(t + \Delta t) = \vec{r}_i(t) - \beta D \Delta t \cdot \nabla_i \Phi_{93}(x_i; s) + \sqrt{2D\Delta t} \cdot \vec{\zeta}. \tag{5}$$

There, $\beta = k_B T^{-1}$ is the inverse thermal energy, D the diffusion coefficient, and $\vec{\zeta}$ a vector of numbers drawn from a Gaussian distribution with mean $\mu = 0$ and variance $\chi = 1$. The internal colloid state s is updated every time step as well. The integration time step for the simulations is typically $\Delta t = 10^{-3}\,\tau$ in units of the Brownian time scale, see below. The switching probabilities are defined by the switching rates $k_{ss'} = k_{ab}, k_{ba}$ through the exponential Poisson form [22]

$$P(s \to s') = 1 - e^{-k_{ss'}(\vec{r},t)\Delta t}. \tag{6}$$

All variables are reduced to characteristic units. Lengths are given in σ, set to unity. Times are measured in the characteristic timescale τ, based on the diffusion coefficient D of the colloids $\tau = \sigma^2/D$. The wall potential uses a cutoff of 4σ in the simulations.

The simulation trajectory is divided into $N_{\mathrm{block}} = 10$ blocks, and the standard errors of block averages based on the standard deviation $\sqrt{\chi_q}$ of a variable q are defined by $f_q = \sqrt{\chi_q}/\sqrt{N_{\mathrm{block}}}$. To gather enough statistics, simulations up to 1000 τ were necessary.

C. Reaction-diffusion Smoluchowski equation

Next to the BD simulations, we describe the colloid behavior by a deterministic theoretical approach. The overdamped dynamics of an ideal gas in an external field is governed by a Fokker-Planck equation, which, in the context of colloid position distributions, is better known as the Smoluchowski diffusion equation [27]. It describes the evolution of the density profiles in state s, $\rho_s(x,t)$, of colloids with diffusion constant D in the external potentials $\Phi_{93}(x;s)$ as a function of time and space. Because the potentials only act in the x direction and equal distributions are expected in y and z, a one-dimensional form is sufficient. We distinguish colloids by their internal state, therefore the system is described by two reaction-coupled Smoluchowski equations [19,28]

as in Eq. (7):

$$\frac{\partial \rho_s(x,t)}{\partial t} = D\frac{\partial^2 \rho_s(x,t)}{\partial x^2} + D\beta\frac{\partial}{\partial x}\left[\rho_s(x,t)\frac{\partial \Phi_{93}(x;s)}{\partial x}\right], \tag{7}$$

for states $s = a, b$ and, for simplicity, D is assumed to be the same for both colloid states. The switching of the internal state introduces a set of coupled differential equations:

$$\frac{\partial \rho_a(x,t)}{\partial t} = -k_{ab}(x,t)\rho_a(x,t) + k_{ba}(x,t)\rho_b(x,t), \tag{8}$$

$$\frac{\partial \rho_b(x,t)}{\partial t} = +k_{ab}(x,t)\rho_a(x,t) - k_{ba}(x,t)\rho_b(x,t). \tag{9}$$

They describe that the density profiles change in time based on the fractions of colloids leaving and entering the respective states. These fractions depend on the switching rates $k_{ss'}$, that are in the most general form time- and space-dependent. In the case of local density dependence, the switching rates are calculated from the current density profile, which introduces this dependency. Combining Eqs. (7)–(9) leads to a system of two second order coupled reaction-diffusion equations, fully describing the colloid behavior through their average densities.

There is no explicit analytical solution for the stationary density distributions $\rho_s(x)$. However, with the stationarity ansatz, $\partial \rho_s(x,t)/\partial t = 0$, the equations simplify and adding the two resulting reaction-diffusion equations further cancels the reactive part. After integrating over dx, a single first order differential equation results (10):

$$\sum_{s=a,b}\left[\frac{\partial \rho_s(x)}{\partial x} + \beta\rho_s(x)\frac{\partial \Phi_{93}(x;s)}{\partial x}\right] = 0. \tag{10}$$

By introducing a new variable, the flux $j(x)$ as the first term of the sum in Eq. (10), the equation can be decoupled and solved for the density profiles $\rho_s(x)$. By deriving an expression for the flux from the initial system of equations, a self-consistent implicit solution is formally found, given by

$$\rho_a(x) = e^{-\beta\Phi_{93}(x;a)}\left[c_a + \int_0^x \frac{j(\tilde{x})}{D}e^{\beta\Phi_{93}(\tilde{x};a)}d\tilde{x}\right], \tag{11}$$

$$\rho_b(x) = e^{-\beta\Phi_{93}(x;b)}\left[c_b - \int_0^x \frac{j(\tilde{x})}{D}e^{\beta\Phi_{93}(\tilde{x};b)}d\tilde{x}\right], \tag{12}$$

$$j(x) = \int_0^x [k_{ab}(\tilde{x})\rho_a(\tilde{x}) - k_{ba}(\tilde{x})\rho_b(\tilde{x})]d\tilde{x}. \tag{13}$$

The integration constants c_a and c_b can be calculated from the conservation condition of a fixed colloid number. We solve this equation system with an iterative procedure, consisting of an initial guess for the density profiles and repeated application of the self-consistent set of equations, until stationary distributions emerge.

There are analytic solutions for the limit of low and fast switching rates, that are connected to our solution. In the low switching rate regime, the flux vanishes and the density profiles recreate the external potentials in an exponential Boltzmann form [19]. Here, the colloids in different states are completely controlled by diffusion. On the contrary, the reactive part of the equations dominates in the fast switching limit, characterised by high switching rates $k_{ss'}$. In this case, colloids of different states are indistinguishable and share a common profile $\rho_a(x) \propto \rho_b(x)$. This ansatz leads again to an exponential Boltzmann form of the resulting density distributions, but with an effective potential given by [19,22]

$$V_{\text{eff}}(x) = \frac{k_{ba}\Phi_{93}(x;a) + k_{ab}\Phi_{93}(x;b)}{k_{ba} + k_{ab}}. \tag{14}$$

Generally, this effective potential depends on the—in general different—diffusion coefficients D_a and D_b of the colloids, but the dependence cancels out in our special case with $D_a = D_b = D$.

D. Measuring local densities

Now we discuss how the local density, $\rho_{\text{loc}}(x)$, can be defined (or physically "measured" by a colloid) in the BD simulations and calculated in the theoretical Smoluchowski description. This is not only of methodical importance for our work, because a sensing colloid (like a cell or bacteria) may also employ different sensing protocols to evaluate the chemical information in the environment. In particular, in what spatial and temporal range it is measured and how the received information is weighted and processed.

To measure $\rho_{\text{loc}}(x)$, we introduce a spherical neighborhood with radius r_{loc} around a colloid. In the discrete-particle simulations, the most intuitive and coarse-grained measurement possibility is then to count and average the number of neighbors N_{near} in this spherical volume and normalize this value by the measurement volume, as given by

$$\rho_{\text{loc}}(\vec{r}) = \frac{\langle N_{\text{near}}(\vec{r})\rangle_{dt_{\text{loc}}}}{\frac{4}{3}\pi r_{\text{loc}}^3} \tag{15}$$

The average is taken over the current and last dt_{loc} time steps, as discussed in more detail below. In reality, cells gain access to their number of neighbors through the concentration of autoinducers in their environment. Since these colloids naturally detect their own autoinducers they themselves are counted in N_{near}, which introduces a minimum local density value $3/(4\pi r_{\text{loc}}^3)$ in the simulation. Reasonable extensions of this definition of ρ_{loc} could also impose a position-dependent weight on the number of colloids that are counted (e.g., colloids in the closer proximity contribute more). The sensing range r_{loc} is a free parameter in our study and systematically scanned from a spatially local to longer-ranged global "sensing." Note that ρ_{loc} is defined to include colloids of both states, hence measures the total density. One could also assume in future work that only one state is sensed and important for response.

Furthermore, we needed to introduce the timescale parameter, dt_{loc}, in the BD simulations which is used to calculate the time average in Eq. (15). It has also a reasonable biological interpretation: The autoinducers need time to diffuse to the cells and be processed at the receptors (which might also need some significant time), while the bacteria move further into other environments. The actual local density inferred by a cell therefore represents an average over a certain timescale. Hence, in the BD simulations we do not restrict ourselves to the instantaneous local density at a given time step, but also include the last dt_{loc} time steps. Therefore, for large dt_{loc}, it increases the precision of the measurement, but the average possibly smears out over the path-dependent history of the

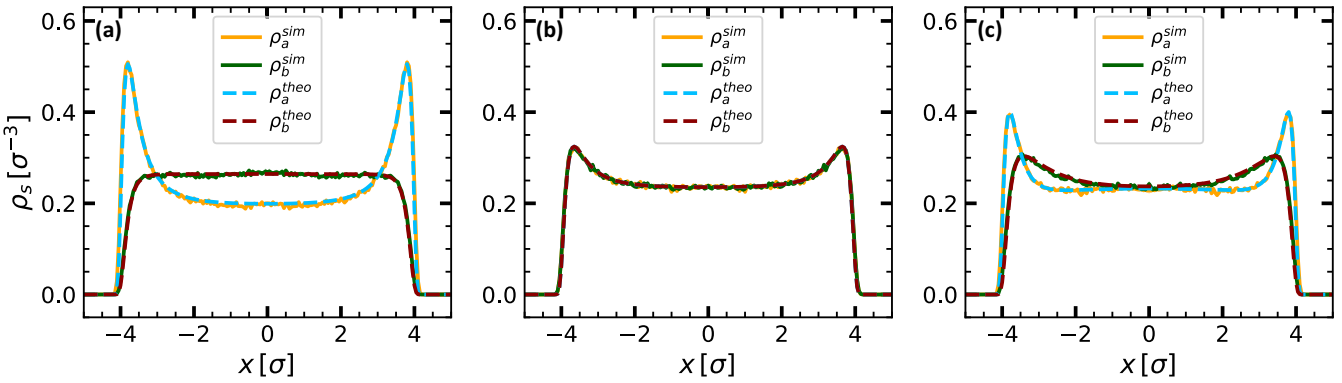

FIG. 3. Density distributions of different simulations with constant switching rates. The results from BD simulations at $\rho_{\text{tot}} = 0.4\sigma^{-3}$ are labeled ρ_s^{sim} and shown as solid lines (orange/light gray and green/dark gray). The theoretical predictions are depicted as dashed lines (blue/light gray and red/dark gray) for both states, respectively. (a) No switching case with $k_{ab} = k_{ba} = 0\,\tau^{-1}$: The distributions mirror the external potentials. (b) Fast switching case with $k_{ab} = k_{ba} = 1000\,\tau^{-1}$: The distributions converge to the same shape, because the fast reactive behavior dominates over the slow diffusion. (c) General switching case with $k_{ab} = k_{ba} = 1\,\tau^{-1}$. The distributions are between the two limits, and neither diffusive nor reactive behavior are dominant.

particle. In the other extreme, if only the instantaneous density would be used, $dt_{\text{loc}} = 0$, the value is highly local in space but prone to fluctuations and maybe of little actual information.

In the theoretical (mean-field) Smoluchowski description only the one-dimensional colloid density profiles are studied in a continuum approach and discrete colloid neighbors cannot be counted in this way, nor their fluctuations. Naturally, the instantaneous position-dependent local density is already provided in the theory as a formal average over an ensemble of particles at fixed time t. The correspondence in the BD simulations would be an average of $\rho_{\text{loc}}(\vec{r})$ for all particles in the simulation box which are in a thin slice at position x and $dt_{\text{loc}} = 0$. However, it is hard to imagine how real cells would agree to such an average. Given the nature of the nonstochastic mean-field approach, the density measure thus cannot be matched to the one in the BD. However, to attempt a connection to the smeared-out average of particles in the radius r_{loc} as in the BD definition, the number of neighbors can be expressed by an integral over the colloid number distribution, and a (weighted) local density defined as

$$\rho_{\text{loc}}(x) = \frac{\int_{x-r_{\text{loc}}}^{x+r_{\text{loc}}} \rho(\tilde{x}) A(\tilde{x})\, d\tilde{x}}{\frac{4}{3}\pi r_{\text{loc}}^3}, \tag{16}$$

where $\rho(x) = \rho_a + \rho_b$ is the self-consistent (total) density distribution from the Smoluchowski theory. Since the colloids are assumed to be equally distributed in the y and z directions, the volume integral can be simplified to a single integral over the x direction. This introduces the area element $A(\tilde{x}) = \pi[r_{\text{loc}}^2 - (\tilde{x} - x)^2]$. Because of the spherical detection range, density values at other positions inside the sphere are also taken into account, but scaled down by the area element weighting factor. Two corrections to Eq. (16) are necessary and included when the sphere intersects the simulation box. First, the integration boundaries can extend outside the box in the x direction and must be capped accordingly. Second, the measurement sphere may extend beyond the simulation box in the y and/or z directions. When it occurs, the area element is no longer spherical but is instead reduced with a maximum calculation of $A(\tilde{x}) = L_y L_z$. We note that we do not attempt to make averages in the Smoluchowski approach over the time-dependent density (i.e., we do not take into account information or "memory" from previous times as provided in the longer dt_{loc} in the BD).

III. RESULTS AND DISCUSSION

A. Constant switching rates

We first demonstrate some representative results for constant (not density-dependent) switching rates, specifically the cases of no switching, fast switching and a general constant rate case with $k_{ab} = k_{ba} = 1\,\tau^{-1}$. The individual theoretical predictions and expectations for these cases and the simulation results are compared in Fig. 3. For all cases, BD simulations and Smoluchowski theory are in perfect agreement, which shows us that both approaches work and can be used to study our quorum sensing model.

Furthermore, the density profiles tell us much about the system. In the no switching case, the profiles mirror the external potentials in the Boltzmann form. State a colloids are attracted to the walls and state b colloids are repelled, so they gather in the center of the simulation box. Because of the short ranged repulsion of the Mie potentials, there is an excluded region near to the walls at positions $\pm 5\,\sigma$, where no colloids can be found at all. As expected and known from previous work on nonideal systems [19], when the switching rates are high ($k_{ab} = k_{ba} = 1000\,\tau^{-1}$) and the fast switching limit is reached, the individual state density profiles take the same form, based on the derived effective potential in Eq. (14). State b colloids are now also gathering at the walls, because they travel to the walls as state a colloids, switch, and then contribute to the density distribution. For intermediate switching rates different density profiles are observed. They interpolate between the two limiting cases and show elements of both distributions. Neither the diffusive, nor the reactive behavior of the colloids are dominant, but both exist at the same time and in constant interplay.

B. Linear rate dependence

We now report the results for the case of switching rates depending linearly on the local density. We first produce

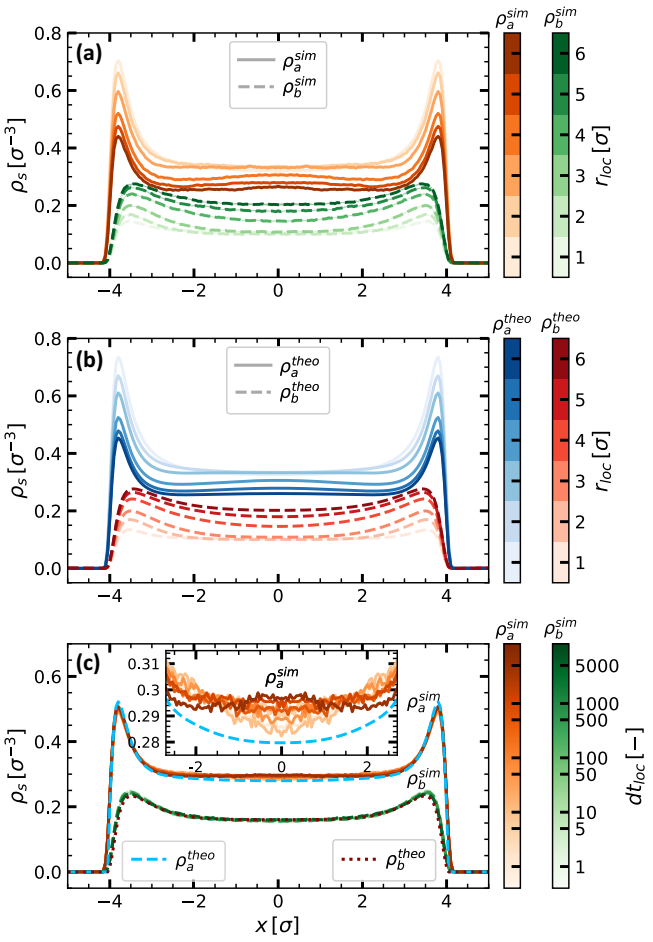

FIG. 4. Influence of the spatiotemporal sensing range parameters r_{loc} and dt_{loc} on the colloid density distributions in the case of a linear rate dependency on local density. The total density is $\rho_{\mathrm{tot}} = 0.4\sigma^{-3}$. (a) BD results for state a (solid lines) and state b (dashed lines). (b) Theoretical predictions for state a (solid lines) and state b (dashed lines). Different parameter values are represented by shades of the same color. Smaller r_{loc} generally lead to stronger position dependence of the local density and therefore to increasingly different switching rates. The number of state a colloids, as well as the adsorption increases. In the limit of infinite r_{loc}, the profiles converge to the constant rate case profiles. (c) Theoretical (dashed lines for ρ_a^{theo} and dotted lines for ρ_b^{theo}) and BD results (solid lines with annotations) depending on dt_{loc}. The time averaging parameter dt_{loc} has only a small effect on the density profiles. For increasing dt_{loc}, a smoothing effect is expected and observed on a small scale, see inset for ρ_a^{sim}.

simulation and theory curves for the individual state density profiles with a linear local density dependence with $k_{\mathrm{init}} = 1\,\tau^{-1}$ and $k_{\mathrm{amp}} = 0.5\,\tau^{-1}$ and varying r_{loc} for $dt_{\mathrm{loc}} = 10$. The profiles are shown in Fig. 4(a) for simulations and Fig. 4(b) for the comparison to the theory.

For very high r_{loc} the measurement sphere contains all of the colloids in the simulation box (including the images) and the local density is therefore constant and converging to the total density, ρ_{tot}. In this limit, the profiles converge to the constant rate case discussed above. In contrast, small r_{loc} values and thus small measurement spheres, lead to a strong position dependence of the local density. Close to the walls, where state a colloids gather due to their attractive behavior, high local densities are measured and the switching rates strongly favor the switching to state a. This leads to high adsorption and a high asymmetry in the colloid numbers of the different states. The density of state a shows high adsorption peaks and the density of state b a flat behavior at small values. The theoretical prediction agrees with the simulation curves perfectly. The results stress how density-dependent interactions (communication) can control the structural and adsorption behavior of the colloids. In particular, the structure can be governed by the colloids by tuning their sensing range, r_{loc}, in space. Large measurement ranges r_{loc} smear out, i.e., homogenize the structure, and return to constant, position-independent switching rates.

In Fig. 4(c) we now consider the influence of varying dt_{loc} for fixed $r_{\mathrm{loc}} = 2\,\sigma$. Different dt_{loc} values somewhat surprisingly show little influence when using a linear density dependence function. Between time averages from 1 up to 5000 time steps, we do not observe significant changes in the behavior. The integration time step for these simulations is $\Delta t = 10^{-3}\,\tau$, so the colloids move by about $5\,\sigma$ during the time averaging. This is expected to result in a smoothing effect, which can be observed only on a small scale in the inset in Fig. 4. Since the effect is small, the colloids apparently do not travel significantly during the time averaging, but stay in their local environment. We suspect that significant contributions to the structure comes from the colloids attracted to the walls, which are quite localized in their diffusion. Because dt_{loc} does not appear in the theoretical Smoluchowski description of our model, a single density profile is provided for the theory for each of the two colloid states, integrated into the figure with dashed lines. Theory and simulations are in good agreement, but show small deviations (less than 5%) in absolute values.

In a similar manner, we studied the influence of the amplitude parameter k_{amp}. The respective simulation and theory profiles for the individual state densities are summarized in Fig. 5. The parameter is varied between $0\,\tau^{-1}$ and $0.8\,\tau^{-1}$. The spatiotemporal sensing range parameters are set to $r_{\mathrm{loc}} = 2\,\sigma$ and $dt_{\mathrm{loc}} = 10$. For a vanishing amplitude, the linear slope is zero and the constant rate case with $k_{ab} = k_{ba} = k_{\mathrm{init}}$ is reached exactly, as evident by comparing the density profiles to Fig. 3. If the amplitude is increased, the impact of the local density dependence increases and state a colloids are favored. Therefore the state profiles diverge from each other and there are more state a colloids in general. The adsorption increases as well, because the position dependence of the local density increases with increasing slope. Especially at the walls, high k_{ba} are reached and colloids of state a cluster. Simulations and theory are in very good agreement and k_{amp}, i.e., the density-dependent magnitude of the switching rate, is identified to have great influence on the colloid structure and the adsorption to a possible biofilm host.

C. Correlation effects for sigmoidal rate dependence

We now turn to the sigmoidal dependence function as described in Eq. (4), in which a critical local density defines the threshold for switching the rate. This introduces two new

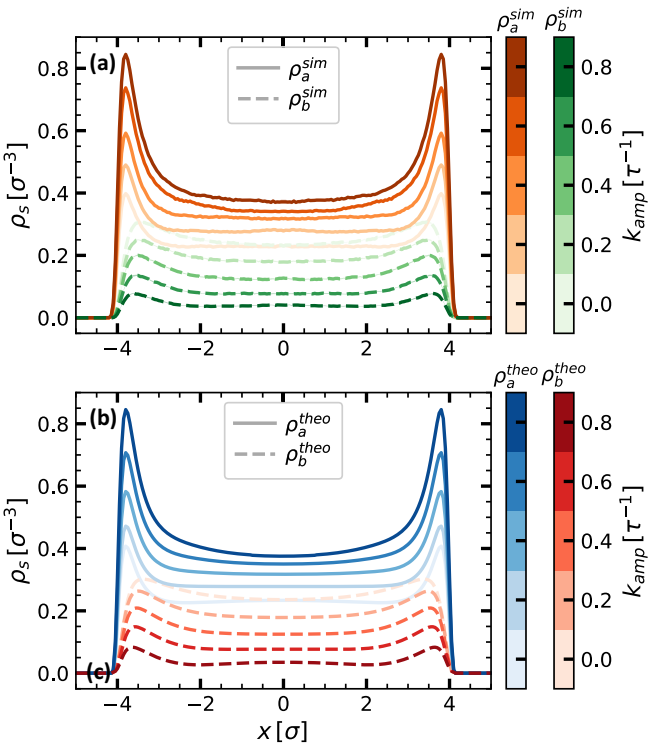

FIG. 5. Influence of the amplitude parameter k_{amp} on the colloid density distributions for the case of the linear rate dependence on local density. The total density is $\rho_{\mathrm{tot}} = 0.4\sigma^{-3}$. (a) BD results for state a (solid lines) and state b (dashed lines). (b) Theoretical predictions for state a (solid lines) and state b (dashed lines). Different parameter values are represented by shades. Smaller k_{amp} recreate the constant rate case with $k_{ab} = k_{ba} = k_{\mathrm{init}}$. High k_{amp} favor switches to state a and the number of state a colloids increases in general. The adsorption also increases, because the position dependence of the local density increases with increasing slope.

parameters, the point of transition ρ_{crit} and its sharpness, controlled by α_{sig}. The latter we set to 50 (with respect to total density), because interesting results are expected with relatively sharp transitions. The critical density is studied in a parameter series and varied in a range of $0.40\,\sigma^{-3}$ to $0.56\,\sigma^{-3}$. The sensing parameters are kept to $r_{\mathrm{loc}} = 2\,\sigma$ and $dt_{\mathrm{loc}} = 10$ first. Figures 6(a) and 6(b) show the simulation density profiles in comparison with the theoretical predictions. Surprisingly, we now observe a strong deviation between simulations and theory. The density distributions in the simulations show a simple trend of favoring state a colloids with decreasing local density. This is because the critical density is exceeded by the local density at many positions and the switching rates are altered, which increases the state a colloid number. A similar trend is also visible in the theoretical density profiles, but for certain intermediate ρ_{crit} values, there are additional structure peaks for both state distributions at $x = \pm 2\,\sigma$.

To investigate the origin of these structure peaks further, the measured local density $\rho_{\mathrm{loc}}(x)$ and the resulting position-dependent switching rates, $k(x)$, for the specific case of $\rho_{\mathrm{crit}} = 0.48\,\sigma^{-3}$ are shown for both theory and simulations in Figs. 6(c) and 6(d), respectively. The adsorption peaks of the particle density $\rho_s(x)$ close to the walls at around $x = \pm 4\,\sigma$ naturally condition the shallow peaks in the local density profiles, $\rho_{\mathrm{loc}}(x)$. However, the peaks are shifted toward the center of the simulation box and appear at around $x = \pm 2\,\sigma$, because a high fraction of the measurement sphere overlaps with the excluded region behind the walls. The spatial distributions of switching rates, $k(x)$, inherit this behavior and show extreme values at $x = \pm 2\,\sigma$, strongly favoring state a colloids. The peak shift is strongly connected to the measurement range r_{loc}; a larger range leads to a stronger shift, because more of the excluded wall region is encapsulated in the measurement sphere. Small r_{loc} push the additional density peaks to the walls until they merge with the attraction peaks at $x = \pm 4\,\sigma$. In the simulation box center, the rates take their initial values, because the decreased local density is below the critical density ρ_{crit}. While the structure in $k(x)$ looks similar for simulations and theory, the local density $\rho_{\mathrm{loc}}(x)$ also differs as for the particle density profiles.

Our further analysis suggests that the origin of the encountered deviation are noise and related measurement fluctuations in the BD simulations. To illustrate this, Fig. 6(e) shows the distributions of measured $\rho_{\mathrm{loc},s}(x = 0)$ for both states s in the center of the simulation box as well as the calculated theoretical values at this position as vertical lines for both states, respectively. The theory has a single value, while the simulation results are distributed in a Gaussian-like fashion. Such a distribution of local densities translates into a corresponding distribution of switching rates. For a linear rate dependence function the mean local density corresponds directly to the switching rates. The sigmoidal shape, however, breaks the direct correspondence between density and local rate distributions and smoothes out the structure peaks in the density profiles of the simulation when based on fluctuating density values. When the local density distribution overlaps with the critical density value, the measured values are translated either into the low or the high switching rate regime, affecting the mean switching rates to not correspond to the mean local density. This is why the structure effect is smoothed out in our BD results for the individual state densities, and they resemble more closely the results obtained with a linear dependence function.

Following this, we pursued possible approaches to manipulate or reduce the fluctuations in the local density measurement in the BD simulations, so that the correlation effect is also visible there. The origin of the measurement uncertainty is generally located in finite and noisy statistics. (Note that a real cell faces the same challenge, i.e., how to process information in the noisy environment.) We conducted simulations with higher overall colloid density of $\rho_{\mathrm{tot}} = 16\,\sigma^{-3}$ to reduce absolute fluctuations in the measurement volume. It is important to note that while increasing the total colloid density is expected to alter the fluctuations in the local density measurement and consequently the shape of the density profile when considering the sigmoidal rate dependence, a change in total colloid density would simply rescales the density profiles accordingly without altering their shape for the other cases. We additionally scanned through different sensing times dt_{loc}. In Fig. 6(f), the density profiles of the different simulations are shown for $r_{\mathrm{loc}} = 2\,\sigma$. Note again, the timescale parameter is not a part of the

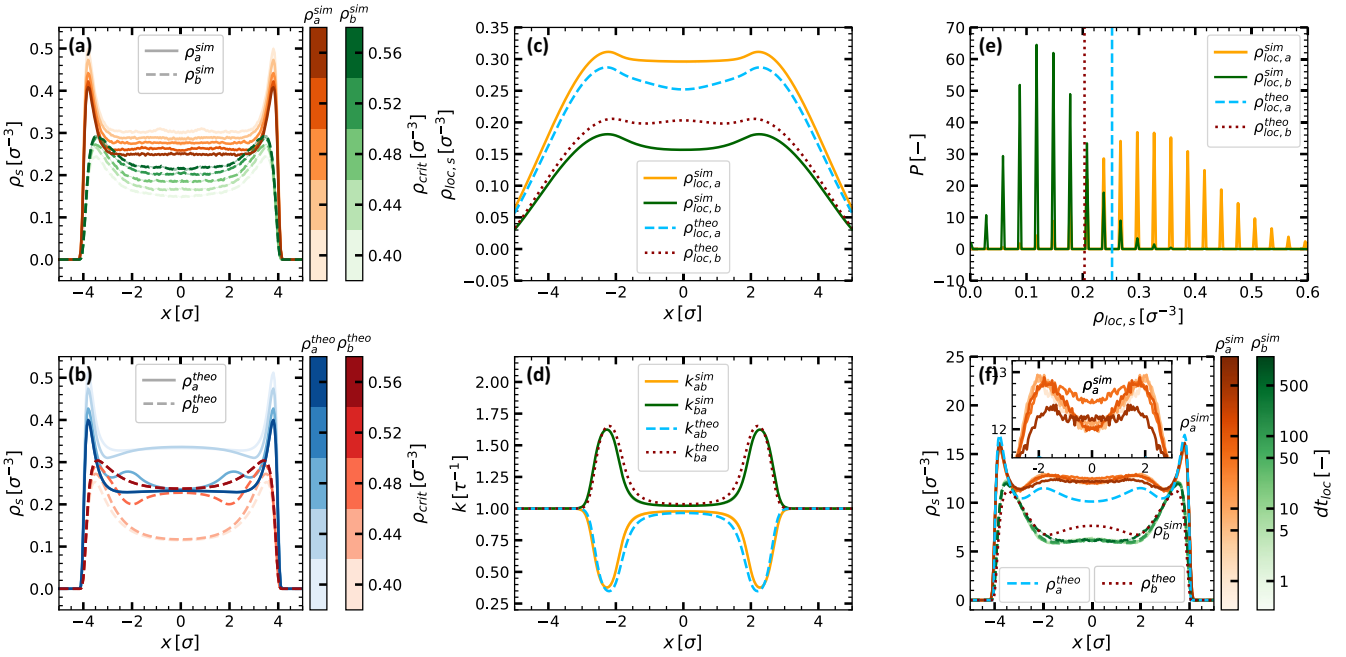

FIG. 6. Structural correlations effects observed for a sigmoidal dependence function. Panels (a) and (b) show density profiles from simulations with varying ρ_{crit}, represented by shades for simulations and theory, respectively. One observes the correlation effect for certain critical densities in the theoretical predictions, but not in the simulation results. Panels (c) and (d) show the local density and the switching rate distributions for an example simulation with $\rho_{\text{crit}} = 0.48\,\sigma^{-3}$. The peaks of the distributions are shifted in comparison to the density peaks, because of the excluded region close to the walls and the finite measurement range. Panel (e) shows the measured local density distributions from the BD simulations and the expected theoretical values in the center of the simulation box. There is a discrepancy, because the fluctuations self consistently affect the colloid behavior. Panel f) shows density distributions of simulations with increased overall density, varying timescale parameter dt_{loc} and fixed $r_{\text{loc}} = 2\,\sigma$. The single theoretical expectations for both states are included as dashed lines for ρ_a^{theo} and dotted lines for ρ_b^{theo}. The structure effect is now visible in the simulation results as well, proving, that it is not just a theoretical artefact.

iteration procedure of the self-consistent Smoluchowski equations, so all simulations share the same theoretical predictions for the density profiles, included as blue and red dashed lines. A slight improvement of the agreement of simulations and theory is visible with increasing dt_{loc}, especially the state a colloid profile in the center of the simulation box shows a deeper local minimum. However, when dt_{loc} is increased to 500, the structure smoothes out, as it averages over the colloidal spatial motion and starts to vanish again. Hence, although the fluctuations can be decreased effectively, the deviation of simulations and theory can never be eradicated, it seems. It is directly coupled to the discrepancy between sharp values in the theory and distributions in the BD simulations. The increased density and the introduction of the timescale parameter dt_{loc}, however, make the correlation effect more apparent in the simulation profiles, proving that the structural effect is not just a theoretical artefact.

IV. CONCLUSION

We studied a system of actively switching binary colloids in an external surface potential. To mimic a quorum sensing type of communication, a local density dependence of the switching rates between the states was imposed. In particular, the colloids were assumed to have two different states a and b, for which the external potentials acted attractively or repulsively, respectively. Otherwise, they were (energetically) noninteracting. We studied this model with Brownian dynamics simulations as well as with a self-consistent set of appropriate reaction-diffusion equations.

In the reference case of constant, position-independent rates, we were able to confirm behavior observed in previous studies of soft colloids [19,22]: Without switching, the density distributions of the colloids of both states just mirror their external potentials in an exponential Boltzmann form, respectively. For high switching rates, the reactive behavior is dominant and the shape of the individual density distributions cannot be distinguished anymore, as described by an effective mixed potential. Intermediate switching rates lead to density profiles extrapolating between these extreme cases.

In the local density-dependent case we first studied a linear dependence function. We conducted parameter studies for the influence of the measurement spatial range and time as well as the rate amplitude. The number of state a colloids and their adsorption to the walls in general is strongly favored by the local density dependence and therefore increase with increasing amplitude as well as with decreasing spatial sensing range. For low amplitudes, the constant rate case is recreated, as well as for infinite radii. The temporal range parameter only showed small influence in these studies, indicating that the colloids do not traverse far away from their local environment of attracting surfaces.

Using a sigmoidal dependence function leads to interesting structural correlation effects in the density distributions. This is remarkable because our colloids are ideal and therefore not

expected to show much structural (such as oscillatory or layering) behavior. It originates purely from their density-mediated communication and is therefore an interesting addition to existing studies. It is generated from an interplay of the external energetic potentials and the finite range, in which the colloids can "sense" the density of other colloids in their environment. However, we did not observe a large correlation effect in the density profiles from the simulation data. There, noise and fluctuations in the local density measurement smooth out the distributions and the structure is suppressed.

As an interesting conclusion of our study we can state that the apparently technical parameters, such as measurement spatial range r_{loc}, temporal range dt_{loc}, amplitude k_{amp}, and threshold density ρ_{crit}, are actually all physical (and biological relevant) sensing parameters. The latter can be used by cells and perhaps synthetic active colloids to tune the communication between them and thus control the collective structure and dynamics of the suspensions.

Our work inspires numerous follow up studies. Methodically, a pressing problem is how to further interpret the fluctuations in the simulation data, because they significantly influence the system. The mean-field Smoluchowski equations do not capture their impact and inclusion of fluctuations might be useful in the theoretical description. Furthermore, the density-dependent switching mediates non-Hamiltonian, nonreciprocal interactions between the particles which in general will violate Newton's third law. Nonreciprocity leads to a rich set of emerging behaviors that are usually hard to account for starting from the microscopic scale, and generic theoretical frameworks out of equilibrium are under development [29–31] and may apply also for quorum sensing interactions. In the context of biofilm formation, our quorum sensing model could be extended to include physical pair interactions [19,20] between the switching colloids, which also switch for different states. Some form of nutrition (or chemical fueling) is also a key element in biofilm research [32], as well as proliferation [33] leading to an increase in total colloid number per time. To consider effects of cell motility, one could also consider self-propelled colloids and related chemotactic or chemophoretic interactions [30,34–39].

Our adsorption studies can be enhanced by including different forms of adhesion [40,41] to the model, possibly realized by sink boundary conditions close to the walls of the simulation. Further understanding the quorum sensing signaling process is key to control it, maybe prevent it when necessary, an approach called antiquorum sensing [42,43]. After all, quorum sensing aids unwanted biofouling and increases resistance to antibiotic treatment. Understanding its role in biofilm formation holds immense potential for the development of novel strategies to combat bacterial infections and enhance various industrial applications.

ACKNOWLEDGMENTS

We thank A. Moncho-Jordá for inspiring discussions. The authors acknowledge support by the state of Baden-Württemberg through bwHPC and the German Research Foundation (DFG) through Grant No. INST 39/963-1 FUGG (bwForCluster NEMO). We also acknowledge the DFG under Germany's Excellence Strategy-EXC-2193/1-390951807.

[1] H. Bartholomew, G. Reynoso, B. Thomas, C. Mullins, C. Smith, I. Gentzel, L. Giese, D. Mackey, and A. Stevens, The transcription factor Lrp of *Pantoea stewartii* subsp. *stewartii* controls capsule production, motility, and virulence important for *in planta* growth, Front. Microbiol. **12**, 806504 (2022).

[2] M. Miller and B. Bassler, Quorum sensing in bacteria, Annu. Rev. Microbiol. **55**, 165 (2001).

[3] C. Waters and B. Bassler, Quorum sensing: Cell-to-cell communication in bacteria, Annu. Rev. Cell Dev. Biol. **21**, 319 (2005).

[4] H. Kaplan and E. Greenberg, Diffusion of autoinducer is involved in regulation of the Vibrio fischeri luminescence system, J. Bacteriol. **163**, 1210 (1985).

[5] M. Montgomery and M. McFall-Ngai, The anatomy and morphology of the adult bacterial light organ of Euprymna scolopes Berry (Cephalopoda:Sepiolidae), Biol. Bull. **179**, 332 (1990).

[6] A. I. Curatolo, N. Zhou, Y. Zhao, C. Liu, A. Daerr, J. Tailleur, and J. Huang, Cooperative pattern formation in multi-component bacterial systems through reciprocal motility regulation, Nat. Phys. **16**, 1152 (2020).

[7] P. Watnick and R. Kolter, Biofilm, city of microbes, J. Bacteriol. **182**, 2675 (2000).

[8] M. Koutsoudis, D. Tsaltas, T. Minogue, and S. Bodman, Quorum-sensing regulation governs bacterial adhesion, biofilm development, and host colonization in *Pantoea stewartii* subspecies *stewartii*, Proc. Natl. Acad. Sci. USA **103**, 5983 (2006).

[9] C. Ratzke, J. Barrere, and J. Gore, Strength of species interactions determines biodiversity and stability in microbial communities, Nat. Ecol. Evol. **4**, 376 (2020).

[10] G. Bixler and B. Bhushan, Review article: Biofouling: Lessons from nature, Phil. Trans. R. Soc. A **370**, 2381 (2012).

[11] Z. K. Zander and M. L. Becker, Antimicrobial and antifouling strategies for polymeric medical devices, ACS Macro Lett. **7**, 16 (2018).

[12] H.-C. Flemming, P. S. Murthy, R. Venkatesan, and K. Cooksey, *Marine and Industrial Biofouling* (Springer-Verlag, Tiergartenstrasse, Heidelberg, Germany, 2009).

[13] J. N. Wilking, T. E. Angelini, A. Seminara, M. P. Brenner, and D. A. Weitz, Biofilms as complex fluids, MRS Bull. **36**, 385 (2011).

[14] U. U. Ghosh, H. Ali, R. Ghosh, and A. Kumar, Bacterial streamers as colloidal systems: Five grand challenges, J. Colloid Interface Sci. **594**, 265 (2021).

[15] A. Boo, R. L. Amaro, and G.-B. Stan, Quorum sensing in synthetic biology: A review, Curr. Opin. Syst. Biol. **28**, 100378 (2021).

[16] H. Qiu, K. Feng, A. Gapeeva, K. Meurisch, S. Kaps, X. Li, L. Yu, Y. K. Mishra, R. Adelung, and M. Baum, Functional polymer materials for modern marine biofouling control, Prog. Polym. Sci. **127**, 101516 (2022).

[17] L. Schimansky-Geier, B. Lindner, S. Milster, and A. B. Neiman, Demixing of two species via reciprocally concentration-dependent diffusivity, Phys. Rev. E **103**, 022113 (2021).

[18] T. Yimyai, R. Thiramanas, T. Phakkeeree, S. Iamsaard, and D. Crespy, Adaptive coatings with anticorrosion and antibiofouling properties, Adv. Funct. Mater. **31**, 2102568 (2021).
[19] A. Moncho-Jordá and J. Dzubiella, Controlling the microstructure and phase behavior of confined soft colloids by active interaction switching, Phys. Rev. Lett. **125**, 078001 (2020).
[20] H. Alston, A. O. Parry, R. Voituriez, and T. Bertrand, Intermittent attractive interactions lead to microphase separation in nonmotile active matter, Phys. Rev. E **106**, 034603 (2022).
[21] D. Zwicker, The intertwined physics of active chemical reactions and phase separation, Curr. Opin. Colloid Interface Sci. **61**, 101606 (2022).
[22] M. Bley, J. Dzubiella, and A. Moncho-Jordá, Active binary switching of soft colloids: Stability and structural properties, Soft Matter **17**, 7682 (2021).
[23] H. Hoang, S. Kang, and Y. Suh, Molecular dynamics study on the effect of solution-wall interaction potential on the properties of solution in uniformly charged hydrophobic channel, J. Mech. Sci. Technol. **24**, 1401 (2010).
[24] P. Kumar, F. W. Starr, S. V. Buldyrev, and H. E. Stanley, Effect of water-wall interaction potential on the properties of nanoconfined water, Phys. Rev. E **75**, 011202 (2007).
[25] U. Baul, N. Göth, M. Bley, and J. Dzubiella, Modulating internal transition kinetics of responsive macromolecules by collective crowding, J. Chem. Phys. **155**, 244902 (2021).
[26] D. Lemons and A. Gythiel, Paul Langevin's 1908 paper "on the theory of Brownian motion," Am. J. Phys. **65**, 1079 (1997).
[27] M. Smoluchowski, Versuch einer mathematischen Theorie der Koagulationskinetik kolloider Lösungen, Z. Phys. Chem. **92**, 129 (1918).
[28] M. te Vrugt and R. Wittkowski, Perspective: New directions in dynamical density functional theory, J. Phys.: Condens. Matter **35**, 041501 (2023).
[29] S. A. Loos and S. H. Klapp, Irreversibility, heat and information flows induced by non-reciprocal interactions, New J. Phys. **22**, 123051 (2020).
[30] A. Dinelli, J. O'Byrne, A. Curatolo, Y. Zhao, P. Sollich, and J. Tailleur, Non-reciprocity across scales in active mixtures, Nat. Commun. **14**, 7035 (2023).
[31] K. L. Kreienkamp and S. H. L. Klapp, Clustering and flocking of repulsive chiral active particles with non-reciprocal couplings, New J. Phys. **24**, 123009 (2022).
[32] E. Giaouris, E. Heir, M. Desvaux, T. Møretrø, S. Langsrud, A. Doulgeraki, G.-J. Nychas, M. Kacaniova, K. Czaczyk, H. Olmez, and M. Simões, Intra- and inter-species interactions within biofilms of important foodborne bacterial pathogens, Front. Microbiol. **6**, 841 (2015).
[33] M. Krsmanovic, D. Biswas, H. Ali, A. Kumar, R. Ghosh, and A. Dickerson, Hydrodynamics and surface properties influence biofilm proliferation, Adv. Colloid Interface Sci. **288**, 102336 (2021).
[34] J. Agudo-Canalejo and R. Golestanian, Active phase separation in mixtures of chemically interacting particles, Phys. Rev. Lett. **123**, 018101 (2019).
[35] F. Fadda, D. A. Matoz-Fernandez, R. van Roij, and S. Jabbari-Farouji, The interplay between chemo-phoretic interactions and crowding in active colloids, Soft Matter **19**, 2297 (2023).
[36] W. J. M. Ridgway, M. P. Dalwadi, P. Pearce, and S. J. Chapman, Motility-induced phase separation mediated by bacterial quorum sensing, Phys. Rev. Lett. **131**, 228302 (2023).
[37] A. Ziepke, I. Maryshev, I. S. Aranson, and E. Frey, Multi-scale organization in communicating active matter, Nat. Commun. **13**, 6727 (2022).
[38] J. Grauer, F. Jan Schwarzendahl, H. Löwen, and B. Liebchen, Optimizing collective behavior of communicating active particles with machine learning, Mach. Learn.: Sci. Technol. **5**, 015014 (2024).
[39] P. Illien and R. Golestanian, Chemotactic particles as strong electrolytes: Debye-Hückel approximation and effective mobility law, J. Chem. Phys. **160**, 154901 (2024).
[40] H. Busscher and H. van der Mei, How do bacteria know they are on a surface and regulate their response to an adhering state? PLoS Pathog. **8**, e1002440 (2012).
[41] M. Katsikogianni and Y. Missirlis, Concise review of mechanisms of bacterial adhesion to biomaterials and of techniques used in estimating bacteria–material interaction, Eur. Cells Mater. **8**, 37 (2005).
[42] E. Paluch, J. Rewak-Soroczyńska, I. Jędrusik, E. Mazurkiewicz, and K. Jermakow, Prevention of biofilm formation by quorum quenching, Appl. Microbiol. Biotechnol. **104**, 1871 (2020).
[43] N. Vasconcelos, J. Croda, and S. Simionatto, Antibacterial mechanisms of cinnamon and its constituents: A review, Microb. Pathogen. **120**, 198 (2018).